IJARCCE ISSN (O) 2278-1021, ISSN (P) 2319-5940

International Journal of Advanced Research in Computer and Communication Engineering

Impact Factor 8.471 ⁜ Peer-reviewed & Refereed journal ⁜ Vol. 15, Issue 8, August 2026

DOI: 10.17148/IJARCCE.2026.15808

Mathematical Modeling of Plasma and Cellular Transport in Pulsatile Arterial Blood Flow

Vishanu Mohan Sharma[1*], Dr. Dileep Singh[2]

Research Scholar, Department of Mathematics, J.S. University, Shikohabad, India[1]

Assistant Professor, Department of Mathematics, J.S. University, Shikohabad, India[2]

Abstract: Blood is a biologically-complex two-phase fluid consisting of suspended cellular (blood) components and plasma. Blood's properties of transport affect the function of the heart while pumping under pulsatile flow conditions. A general and total analytical model for plasma transport and blood-cell transport through a cylindrical artery experiencing pulsatile pressure drops is developed. Equations used for developing the model are the incompressible Navier-Stokes equations with viscosity depending on hematocrit (the volume fraction of red blood cells), a convective-diffusive-migrative equation describing cellular transport, and an advective-diffusive equation describing plasma solute transport. Analytical solutions for the parameters are determined by separating variables and solving them using the axisymmetric fully developed pulsatile flow analytical solution of Womersley. In addition to giving the spatial distributions of velocity, hematocrit, plasma concentration, cellular concentration, wall shear stress, and volumetric flow rate the solutions provide information concerning changes that occur due to varying hematocrit levels. Numerical simulation results indicate that higher hematocrit values result in increased effective viscosity of blood. Increased blood viscosity causes decreased velocities in the direction of flow, decreases the maximum flow rates occurring during the pulse cycle, and increases frictional resistance to flow. Additionally, numerical simulation results demonstrate the existence of a "cell-rich core" along the centerline of vessels and a "plasma-depleted zone" near vessel walls. These zones develop because shear-induced migration of red blood cells towards the centerline. Plasma concentration decreases continuously downstream from the inlet due to a combination of advection, diffusion, and wall transport.

Keywords: Pulsatile blood flow, Plasma transport, Cellular transport, Hematocrit, Mathematical modeling, Non-Newtonian blood

I. INTRODUCTION

The vascular circulation has an important role in supplying tissue/organ oxygenation and exchange of nutrients as well as cardiovascular performance. Blood is a non-Newtonian suspension. Plasma provides the primary medium for transporting cellular components. Red blood cells are the primary cellular component. The interaction of the two phases may significantly influence the viscosity of blood, the amount of resistance that exists to the flow of blood and importantly, the ability of mass transfer to occur across the vessel walls due to flow generated from the rhythmic pulsatility of the heart. Changes in hematocrit cause corresponding changes in the rheologic properties of blood which lead to changes in velocity distributions, wall shear stress and ultimately transport of dissolved biochemicals. Therefore, understanding both the individual and combined mechanisms responsible for transport of plasma and cellular components is critical for describing either normal or pathologically altered hemodynamics. Accordingly, a theoretical model was developed to simulate plasma and cellular transport in arteries during the pulsatile flow of blood utilizing incompressible Navier-Stokes equations for simulating blood flow and coupled convection-diffusion equations for simulating plasma solute transport and hematocrit migration. It is further assumed that the effective viscosity of blood depends upon hematocrit. Shear-induced migration is further used to represent the migration of red blood cells from regions of high shear rate to regions of low shear rate. Solutions were found analytically under axisymmetric conditions assuming fully-developed flow so as to obtain analytical solutions for predicting velocity profiles; hematocrit distribution; plasma concentrations; cellular concentrations; wall shear stresses; and pulsatile flow characteristics. This proposed model offers a comprehensive theoretical framework for studying the effects of hematocrit upon arterial hemodynamics and plasma-cell interactions.

Akbar *et al.* (2016) studied rheological characteristics of blood using the Reiner Rivlin fluid model in tapered arteries with stenosis. Analytically they showed that tapering arterial structure strongly changes velocity distribution, pressure gradient and wall shear stress. They report that increasing degree of stenosis greatly increases resistance to flow and reduces volume flow rate and that blood's non Newtonian nature becomes increasingly important under severe constriction. Results established that accurate characterization of rheology is essential for realistic prediction of

DOI: 10.17148/IJARCCE.2026.15808

hemodynamics in arteries. **Bessonov *et al.* (2016)** review comprehensively diverse mathematical methods used for modeling blood flow at different spatial and temporal scales. They discuss one dimensional, two dimensional, three dimensional approaches as well as particle based and multiscale computational methods and stress that no single mathematical model adequately represents all physiological conditions. Their work stresses coupling fluid dynamics with mechanics of vessel walls, transport of biochemistry and cellular interactions for realistic cardiovascular simulations. This review sets theoretical foundation for many subsequent computational studies. **Ahmad *et al.* (2019)** analyzed steady blood flow through tapered asymmetric arteries using power law fluid model. Analytical results showed that both taper angle and geometry of stenosis strongly influence velocity profiles and pressure drop. Results showed that asymmetries generate much more complex flow fields compared to symmetric constriction and substantially increase resistance to flow. Results emphasized that arterial geometry must be modeled accurately when developing predictive hemodynamic models. **Abidin *et al.* (2021)** further analyzed blood flow incorporating Herschel Bulkley rheology along with chemical reactions and dispersion of solutes. Results showed yield stress characteristics strongly influence solute transport in stenosed arteries. They observed that stronger reactions reduce solute concentration and rheological parameters affect dispersion patterns. Results also highlight importance of simultaneously considering fluid rheology and biochemical transport in cardiovascular disease modeling. **Ahmad *et al.* (2021)** used Carreau non Newtonian fluid model to study blood flow through arteries with nonlinear tapering. Their analytical formulation showed that shear thinning modifies velocity distribution and wall shear stress as well as pressure gradient very differently from simpler rheological models. **Ali *et al.* (2021)** performed a detailed parametric study of blood flow through arteries with stenosis using mathematical modeling techniques. They systematically looked into height of stenosis, geometry of the vessel and rheological parameters and their effect on drop in pressure and shear stress at the wall. Analysis showed that severity of stenosis greatly increases resistance to flow and reduces axial velocity. Results provided important quantitative relationships between geometric features and hemodynamic variables. **Zhang *et al.* (2023)** numerically studied migration of red blood cells in microvascular bifurcations. Simulations showed that bifurcation geometry strongly influences distribution of cells and partitioning of hematocrit and skimming of plasma. They showed red blood cells preferentially migrate toward larger daughter branches leading to heterogeneity downstream. These results highlighted that cellular migration should be considered when studying micro circulation and oxygen transport. **Riahi and Orizaga (2024)** developed mathematical formulations describing arterial blood flow along with solute transport under conditions of atherosclerosis. Their work showed that narrowing of arteries modifies concentration gradients and efficiency of transport alongside changes in velocity and pressure fields. They stressed coupling fluid mechanics with biochemical transport mechanisms is important for understanding progression of disease and delivery of therapy. **Ahmed *et al.* (2025)** reviewed recent mathematical models developed for flow in the aorta and coronary arteries. They compared analytical, numerical and computational approaches used for hemodynamics of large vessels and stressed growing role of personalized modeling. Their review concluded combining advanced computational techniques with medical imaging significantly improves prediction of cardiovascular disease and supports clinical decisions. **Kumar and Sharma (2025)** summarize evolution of non Newtonian mathematical models applied to flow in stenosed arteries. Researchers critically compared rheological models such as Newtonian, Casson, Carreau, Herschel Bulkley, Power Law, and Cross and others and showed that viscosity that varies with shear stress performs much better physiologically compared to assuming Newtonian behavior. They concluded that choosing an appropriate constitutive model is important to make reliable predictions of pressure gradient, wall shear stress and velocity distribution. **Reddy *et al.* (2025)** introduced dual rheology finite element framework to simulate blood flow through arteries with nanostent stenosis. Simulations showed incorporating dual rheology improves prediction of recirculation flow, shear stress and drug transport. They also showed optimized stent designs reduce adverse hemodynamics while enhancing localized drug delivery and support more effective cardiovascular interventions. **Hussain *et al.* (2026)** also studied blood flow through arteries that have both stenosis and dilation using computational fluid dynamics. Numerical analysis showed alternating narrowing and expansion creates highly complex flow structures with recirculation zones, fluctuations in pressure and peaks of localized shear stress. **Kim *et al.* (2026)** showed that dilation modifies hemodynamics downstream and they advocate incorporating this into realistic models of arterial disease. They developed an efficient framework for personalized arterial simulations using smoothed particle hydrodynamics. Their method captured interaction between pulsatile blood flow and deformable arterial walls while reducing computational cost compared to conventional approaches. Results showed improved numerical stability and enhanced capability for realistic cardiovascular biomechanics in complex arterial shapes. **Okafor *et al.* (2026)** studied magnetohydrodynamics of blood flow through channels with porous atherosclerosis and considered temperature variation and elevated sickle cell concentration. Mathematical analysis showed that increasing sickling concentration greatly increases viscosity and resistance while magnetic intensity suppresses fluid velocity. They concluded that thermal effects, characteristics of porous media and disorders of blood cells all have significant influence on hemodynamics in arteries. **Zhao (2026)** reviews recent developments relevant to biomedical engineering in dynamics of pulsatile blood flow. This study stresses the importance of transient flow behavior, propagation of pressure waves, arterial compliance and complex rheological effects when modeling cardiovascular systems. Results show that more

International Journal of Advanced Research in Computer and Communication Engineering
Impact Factor 8.471 ⁜ Peer-reviewed & Refereed journal ⁜ Vol. 15, Issue 8, August 2026
DOI: 10.17148/IJARCCE.2026.15808

realistic pulsatile simulations yield better prediction of wall shear stress and oscillatory shear index and also improve assessment of diseases and design of biomedical devices compared to steady flow approximations.

II. MATHEMATICAL FORMULATION

Consider an incompressible, pulsatile, two-component blood flow through a cylindrical artery of radius R and length L. Blood is modeled as a suspension of plasma and cellular components, mainly red blood cells. The cellular concentration is represented by the local hematocrit $H(x,t)$. Continuum RBC/hematocrit transport models and convection–diffusion models are commonly used for macroscopic blood-flow transport studies.

2.1. Geometry and Flow Domain:

Let $\Omega = \{(r,z): 0 \le r \le R, 0 \le z \le L\}$ (1)

where r is the radial coordinate and z is the axial coordinate. The velocity field is $u = (u_r, u_z)$

pressure is p, plasma solute concentration is C_p, and cellular volume fraction is H.

2.2. Continuity Equation: For incompressible blood flow,

$\nabla . u = 0$ (2)

In cylindrical coordinates,

$\frac{1}{r}\frac{\partial}{\partial r}(ru_r) + \frac{\partial u_z}{\partial z} = 0$ (3)

2.3. Momentum Equation for Pulsatile Blood Flow: The governing Navier–Stokes equation is

$\rho\left(\frac{\partial \mathbf{u}}{\partial t} + \mathbf{u}.\nabla\mathbf{u}\right) = -\nabla p + \nabla.\tau$ (4)

where ρ is blood density and τ is the viscous stress tensor:

$\tau = \mu_{eff}(H,\dot{\gamma})[\nabla \boldsymbol{u} + (\nabla \boldsymbol{u})^{T}]$ (5)

The effective viscosity depends on hematocrit and shear rate:

$\mu_{eff} = \mu_p f(H,\dot{\gamma})$ (6)

where μ_p is plasma viscosity. A simple hematocrit-dependent model may be written as

$\mu_{eff} = \mu_p(1 + \alpha H + \beta H^2)$ (7)

where α and β are empirical constants. More advanced models may include the Fåhræus–Lindqvist effect, where apparent viscosity depends on vessel diameter and hematocrit.

2.4. Pulsatile Pressure Gradient: The pulsatile driving force is imposed as

$-\frac{\partial p}{\partial z} = G_0 + G_1 cos(\omega t)$ (8)

where G_0 is the steady pressure-gradient component, G_1 is the pulsatile amplitude, and $\omega = 2\pi f$ is the angular frequency.

IJARCCE ISSN (O) 2278-1021, ISSN (P) 2319-5940

International Journal of Advanced Research in Computer and Communication Engineering

Impact Factor 8.471 ⁜ Peer-reviewed & Refereed journal ⁜ Vol. 15, Issue 8, August 2026

DOI: 10.17148/IJARCCE.2026.15808

Thus, $\rho \frac{\partial u_z}{\partial t} = -\frac{\partial p}{\partial z} + \frac{1}{r}\frac{\partial}{\partial r}\left(r\mu_{eff}\frac{\partial u_z}{\partial r}\right)$ (9)

2.5. Cellular Transport Equation: The local hematocrit satisfies an advection–diffusion–migration equation:

$$\frac{\partial \mathrm{H}}{\partial \mathrm{t}} + \mathbf{u}.\nabla \mathrm{H} = \nabla.(\mathrm{D_H}\nabla \mathrm{H}) - \nabla.(\mathbf{V_m}\mathrm{H}) \quad (10)$$

where $\mathrm{D_H}$ is the cellular dispersion coefficient and $\mathbf{V_m}$ is the shear-induced migration velocity. A commonly used form is

$$\mathbf{V_m} = -\mathrm{k_m}\nabla\dot{\gamma} \quad (11)$$

where $\mathrm{k_m}$ is the migration coefficient and $\dot{\gamma}$ is the shear rate.

The shear rate is $\dot{\gamma} = \sqrt{2\mathrm{D}:\mathrm{D}}$ with $\mathbf{D} = \frac{1}{2}[\nabla\mathbf{u} + (\nabla\mathbf{u})^{\mathbf{T}}]$ (12)

2.6. Plasma Solute Transport Equation: For a plasma-borne solute,

$$\frac{\partial C_p}{\partial t} + \mathbf{u}.\nabla \mathrm{C_p} = \nabla.\left(\mathrm{D_p}\nabla \mathrm{C_p}\right) - \mathrm{k_a}\mathrm{C_p} + \mathrm{S_p} \quad (13)$$

where $\mathrm{C_p}$ is plasma concentration, $\mathrm{D_p}$ is plasma diffusivity, $\mathrm{k_a}$ is absorption or reaction rate, and $\mathrm{S_p}$ is a source term. Advection–diffusion transport is standard in arterial solute-transport modeling.

2.7. Coupling Between Plasma and Cells: If the transported species exchanges between plasma and cellular phase, introduce cellular concentration C_c:

$$\frac{\partial C_c}{\partial t} + \mathbf{u}.\nabla \mathrm{C_c} = \nabla.(\mathrm{D_c}\nabla \mathrm{C_c}) + \mathrm{k_{pc}}\mathrm{C_p} - \mathrm{k_{cp}}\mathrm{C_c} \quad (14)$$

The exchange between plasma and cells is $S_{pc} = k_{pc}C_p - k_{cp}C_c$

Thus, $\mathrm{S_p} = -S_{pc}$ (15)

2.8. Boundary Conditions: At the arterial wall $r = R$: $u_r = 0, u_z = 0$

For cellular transport, $\frac{\partial H}{\partial r} = 0$ (16)

For plasma solute transport, $-D_p\frac{\partial C_p}{\partial r} = k_w C_p$ (17)

where k_w is the wall uptake coefficient.

At the centerline $r = 0$: $\frac{\partial u_z}{\partial r} = 0, u_r = 0, \frac{\partial H}{\partial r} = 0, \frac{\partial C_p}{\partial r} = 0$ (18)

At the inlet $z = 0$:

$$u_z(r,t) = U_0(1 + \varepsilon sin\omega t)\left(1 - \frac{r^2}{R^2}\right) \quad (19)$$

At the outlet $z = L$: $p = p_{out}$

$$\frac{\partial H}{\partial z} = 0, \frac{\partial C_p}{\partial z} = 0 \quad (20)$$

International Journal of Advanced Research in Computer and Communication Engineering
Impact Factor 8.471 ⁜ Peer-reviewed & Refereed journal ⁜ Vol. 15, Issue 8, August 2026
DOI: 10.17148/IJARCCE.2026.15808

2.9. Non-Dimensional Parameters:

Use $r^* = \frac{r}{R}, z^* = \frac{z}{L}, t^* = \omega t, u^* = \frac{\boldsymbol{u}}{U_0}$ (21)

Important dimensionless numbers are:

$$Re = \frac{\rho U_0 R}{\mu_0}, W_O = R\sqrt{\frac{\rho\omega}{\mu_0}}, P_{e_p} = \frac{U_0 R}{D_p}, P_{e_H} = \frac{U_0 R}{D_H}, Da = \frac{k_w R}{D_p} \quad (22)$$

Here Re is the Reynolds number, W_0 is the Womersley number, P_{e_p} is the plasma solute Peclet number, P_{e_H} is the cellular Peclet number, and D_a is the wall uptake Damköhler number.

III. SOLUTION OF THE MATHEMATICAL MODEL

Assume axisymmetric, fully developed pulsatile flow: $u_r = 0, u_z = u(r,t), p = p(z,t)$ (23)

And $-\frac{\partial p}{\partial z} = G_0 + G_1 \cos(\omega t)$ (24)

3.1. Velocity Solution: The axial momentum equation becomes

$$\rho\frac{\partial u}{\partial t} = G_0 + G_1\cos(\omega t) + \frac{1}{r}\frac{\partial}{\partial r}\left(r\mu_{eff}\frac{\partial u}{\partial r}\right) \quad (25)$$

For constant effective viscosity $\mu_{eff} = \mu_0$,

$$\rho\frac{\partial u}{\partial t} = G_0 + G_1\cos(\omega t) + \frac{\mu_0}{r}\frac{\partial}{\partial r}\left(r\frac{\partial u}{\partial r}\right)$$

The solution is written as $u(r,t) = u_s(r) + u_p(r,t)$

where u_s is the steady Poiseuille part and u_p is the oscillatory part.

The steady solution is $u_s(r) = \frac{G_0}{4\mu_0}(R^2 - r^2)$

The pulsatile solution is $u_p(r,t) = \Re\left[\frac{G_1}{i\omega\rho}\left\{1 - \frac{J_0(\lambda r)}{J_0(\lambda R)}\right\}e^{i\omega t}\right]$

Where $\lambda^2 = \frac{i\omega\rho}{\mu_0}$

and J_0 is the Bessel function of the first kind.

Thus, the complete velocity field is

$$u(r,t) = \frac{G_0}{4\mu_0}(R^2 - r^2) + \Re\left[\frac{G_1}{i\omega\rho}\left\{1 - \frac{J_0(\lambda r)}{J_0(\lambda R)}\right\}e^{i\omega t}\right] \quad (26)$$

This is the classical Womersley-type velocity solution.

3.2. Shear Rate Solution: The shear rate is $\dot{\boldsymbol{\gamma}}(\boldsymbol{r},\boldsymbol{t}) = \left|\frac{\partial \boldsymbol{u}}{\partial \boldsymbol{r}}\right|$

Therefore, $\frac{\partial u_s}{\partial r} = -\frac{G_0 r}{2\mu_0}$

IJARCCE ISSN (O) 2278-1021, ISSN (P) 2319-5940

International Journal of Advanced Research in Computer and Communication Engineering

Impact Factor 8.471 ⁜ Peer-reviewed & Refereed journal ⁜ Vol. 15, Issue 8, August 2026

DOI: 10.17148/IJARCCE.2026.15808

For the pulsatile part,

$$\frac{\partial u_p}{\partial r} = \Re\left[\frac{G_1 \lambda J_1(\lambda r)}{i\omega\rho J_0(\lambda R)} e^{i\omega t}\right]$$

Hence, $\dot{\boldsymbol{\gamma}}(\boldsymbol{r}, \boldsymbol{t}) = -\frac{G_0 r}{2\mu_0} + \Re\left[\frac{G_1 \lambda J_1(\lambda r)}{i\omega\rho J_0(\lambda R)} e^{i\omega t}\right]$ (27)

3.3. Hematocrit Transport Solution: The cellular transport equation is

$$\frac{\partial H}{\partial t} + u(r,t)\frac{\partial H}{\partial z} = D_H\left[\frac{1}{r}\frac{\partial}{\partial r}\left(r\frac{\partial H}{\partial r}\right) + \frac{\partial^2 H}{\partial z^2}\right] - \nabla.(\nabla_m H)$$

For weak radial migration, take $\nabla_m \approx 0$

Then, $\frac{\partial H}{\partial t} + u(r,t)\frac{\partial H}{\partial z} = D_H\left[\frac{1}{r}\frac{\partial}{\partial r}\left(r\frac{\partial H}{\partial r}\right) + \frac{\partial^2 H}{\partial z^2}\right]$

For high Peclet number flow, axial diffusion is neglected:

$$\frac{\partial H}{\partial t} + u(r,t)\frac{\partial H}{\partial z} = D_H\frac{1}{r}\frac{\partial}{\partial r}\left(r\frac{\partial H}{\partial r}\right)$$

Using separation of variables,

$$H(r,z,t) = H_0 + \sum_{n=1}^{\infty} A_n J_0\left(\frac{\alpha_n r}{R}\right) exp\left[-\frac{D_H {\alpha_n}^2 t}{R^2}\right]$$

where α_n are roots satisfying the wall condition $J_1(\alpha_n) = 0$

If axial convection is retained, use the characteristic transformation

$$z^* = z - \int_0^t u(r,\tau)d\tau$$

Then, $H(r,z,t) = H_0 + \sum_{n=1}^{\infty} A_n J_0\left(\frac{\alpha_n r}{R}\right) exp\left[-\frac{D_H {\alpha_n}^2 t}{R^2}\right] F\left(z - \int_0^t u(r,\tau)d\tau\right)$ (28)

3.4. Plasma Solute Transport Solution: The plasma concentration equation is

$$\frac{\partial C_p}{\partial t} + u(r,t)\frac{\partial C_p}{\partial z} = D_p\left[\frac{1}{r}\frac{\partial}{\partial r}\left(r\frac{\partial C_p}{\partial r}\right) + \frac{\partial^2 C_p}{\partial z^2}\right] - \mathrm{k_{pc}C_p} + \mathrm{k_{cp}C_c}$$

For weak plasma-cell exchange, $\mathrm{k_{pc}}, \mathrm{k_{cp}} \approx 0$

Then,

$$\frac{\partial C_p}{\partial t} + u(r,t)\frac{\partial C_p}{\partial z} = D_p\left[\frac{1}{r}\frac{\partial}{\partial r}\left(r\frac{\partial C_p}{\partial r}\right)\right]$$

The solution is

$$C_p(r,z,t) = C_{p0} + \sum_{n=1}^{\infty} B_n J_0\left(\frac{\beta_n r}{R}\right) exp\left[-\frac{D_p {\beta_n}^2 t}{R^2}\right] G\left(z - \int_0^t u(r,\tau)d\tau\right)$$

where β_n are Eigen values determined from the wall condition.

For zero-flux wall condition, $\frac{\partial C_p}{\partial r} = 0 \Longrightarrow J_1(\beta_n) = 0$

IJARCCE ISSN (O) 2278-1021, ISSN (P) 2319-5940

International Journal of Advanced Research in Computer and Communication Engineering

Impact Factor 8.471 ⁜ Peer-reviewed & Refereed journal ⁜ Vol. 15, Issue 8, August 2026

DOI: 10.17148/IJARCCE.2026.15808

For wall uptake, $-D_p \frac{\partial C_p}{\partial r} = k_w C_p$ the Eigen values satisfy

$$D_p \beta_n J_1(\beta_n) = k_w R J_0(\beta_n) \tag{29}$$

3.5. Cellular-Phase Solute Solution: The cellular concentration equation is

$\frac{\partial C_c}{\partial t} + u(r,t)\frac{\partial C_c}{\partial z} = D_c \nabla^2 C_c + \mathrm{k_{pc}C_p} - \mathrm{k_{cp}C_c}$

Along a streamline, $\frac{\partial C_c}{\partial t} = \mathrm{k_{pc}C_p} - \mathrm{k_{cp}C_c}$

If $\mathrm{C_p}$ is known, then

$$C_c(t) = C_c(0) + \mathrm{k_{pc}} \int_0^t \mathrm{C_p}(\tau) \mathrm{e}^{-\mathrm{k_{cp}}(\mathrm{t}-\tau)}\ \mathrm{d}\tau \tag{30}$$

This gives the cellular uptake of plasma species.

3.6. Wall Shear Stress: Wall shear stress is

$\tau_w(t) = \mu_{eff} \frac{\partial u}{\partial r}\Big|_{r=R}$

Therefore,

$$\tau_w(t) = \mu_0 \left[-\frac{G_0 R}{2\mu_0} + \Re\left(\frac{G_1 \lambda J_1(\lambda r)}{i\omega\rho J_0(\lambda R)} e^{i\omega t} \right) \right]$$

or

$$\tau_w(t) = -\frac{G_0 R}{2} + \mu_0 \Re\left(\frac{G_1 \lambda J_1(\lambda r)}{i\omega\rho J_0(\lambda R)} e^{i\omega t} \right) \tag{31}$$

IV. Results and Discussion

The developed mathematical model is numerically evaluated using physiologically relevant arterial and blood parameters to investigate the influence of hematocrit on pulsatile plasma and cellular transport. The simulation results include axial velocity profiles, temporal variation of peak velocity and flow rate, hematocrit redistribution, plasma concentration, cellular concentration, and wall shear stress under different hematocrit conditions. The graphical outcomes also show how an increase in hematocrit has an influence on the properties of blood's rheological behavior by causing the viscosity to be increased; thus, decreasing the speed and volume rate of blood as well as the resistance against which it flows. In addition, the simultaneous solutions to the coupled transport equations are able to describe the development of a cell-dense central core and a peripheral layer depleted with respect to plasma resulting from red blood cells' movement toward the lower-shear regions caused by the convective, diffusive and transverse transport of the cells. The plasma concentration continues to decrease along the artery length due to convection, diffusion, and wall transport. However, the concentration of cells continues to increase along the artery length as a result of the redistribution of the suspended cells within the artery.

Table 6.1: Simulation Parameters

Parameter	Symbol	Value
Artery radius	R	0.003 m
Artery length	L	0.06 m
Blood density	ρ	1060 kg/m³
Plasma viscosity	μ_p	0.0012 Pa·s
Hematocrit	H_0	0.45

IJARCCE ISSN (O) 2278-1021, ISSN (P) 2319-5940

International Journal of Advanced Research in Computer and Communication Engineering

Impact Factor 8.471 ⁜ Peer-reviewed & Refereed journal ⁜ Vol. 15, Issue 8, August 2026

DOI: 10.17148/IJARCCE.2026.15808

Pulse frequency	f	1.2 Hz
Plasma diffusivity	D_p	10^{-10} m²/s
Cellular diffusivity	D_H	5×10^{-11} m²/s

Table 6.2: Numerical Results Obtained

Quantity	**Numerical value**
Effective viscosity (μ_{eff})	0.00498 $Pa.s$
Minimum peak velocity	0.2713 m/s
Maximum peak velocity	0.8132 m/s
Final peak velocity	0.7929 m/s
Minimum wall shear stress	-2.6999 Pa
Maximum wall shear stress	-0.9006 Pa
Final wall shear stress	-2.6326 Pa
Minimum flow rate	3.834×10^{-6} m³/s
Maximum flow rate	1.149×10^{-5} m³/s
Final flow rate	1.121×10^{-5} m³/s
Hematocrit range	0.4286 to 0.4716
Mean hematocrit	-0.4634
Plasma concentration range	0.9512 to 1.1348
Mean plasma concentration	-0.9948

IJARCCE ISSN (O) 2278-1021, ISSN (P) 2319-5940

International Journal of Advanced Research in Computer and Communication Engineering

Impact Factor 8.471 ⁜ Peer-reviewed & Refereed journal ⁜ Vol. 15, Issue 8, August 2026

DOI: 10.17148/IJARCCE.2026.15808

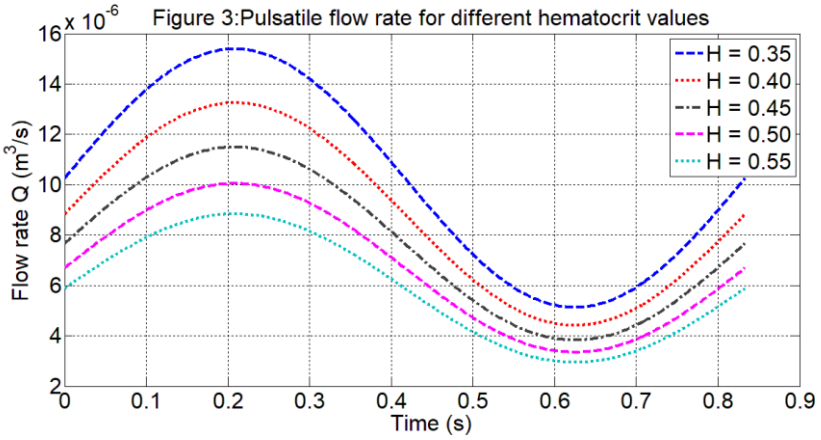

Figure 3:Pulsatile flow rate for different hematocrit values

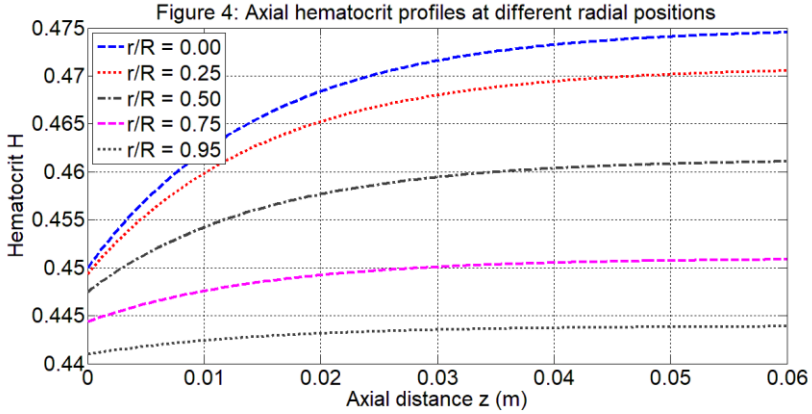

Figure 4: Axial hematocrit profiles at different radial positions

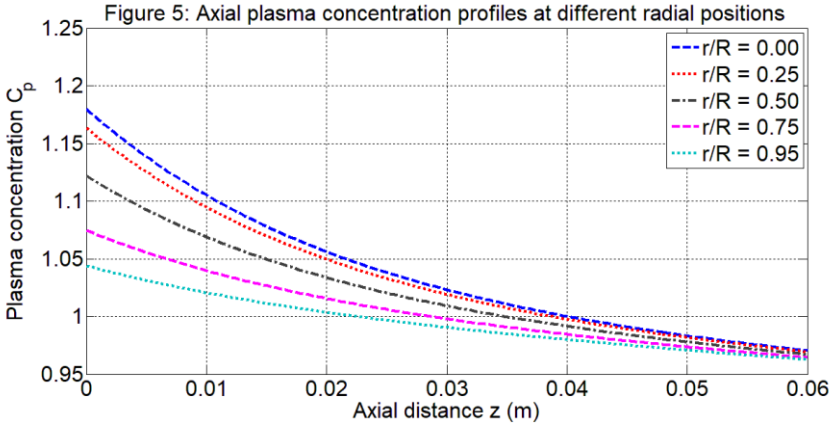

Figure 5: Axial plasma concentration profiles at different radial positions

IJARCCE ISSN (O) 2278-1021, ISSN (P) 2319-5940

International Journal of Advanced Research in Computer and Communication Engineering

Impact Factor 8.471 ⁜ Peer-reviewed & Refereed journal ⁜ Vol. 15, Issue 8, August 2026

DOI: 10.17148/IJARCCE.2026.15808

Figure 6: Axial cellular concentration profiles at different radial positions

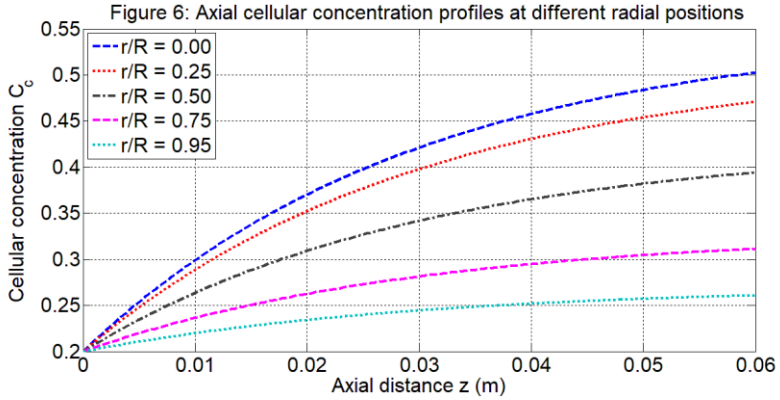

Figure 7: Radial hematocrit profiles at different axial locations

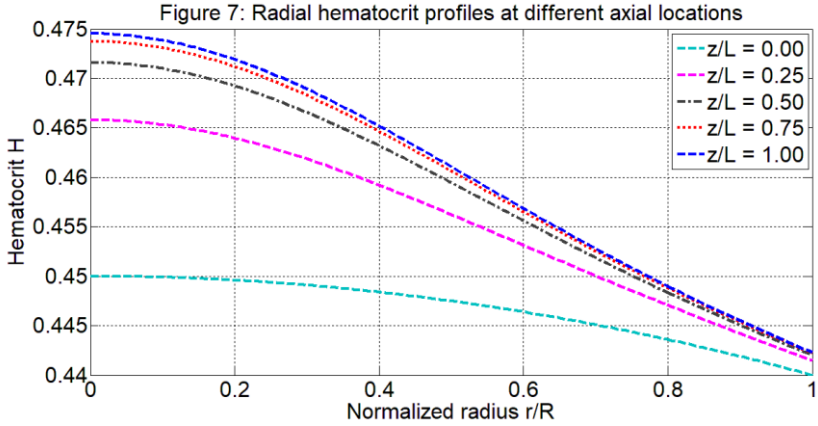

Figure 8: Axial plasma concentration profiles at different radial positions

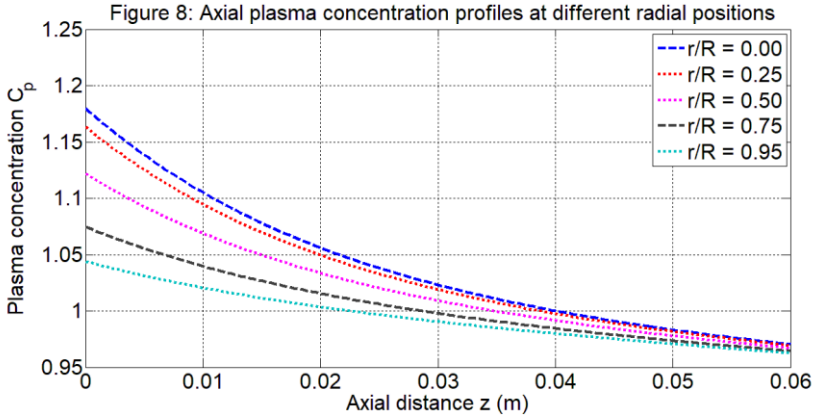

The data presented in figure (1) indicate how the axial velocity profile changes along the diameter of an artery when it is subjected to pulsatile flow at different hematocrits. The x-axis is centered around the center line of the artery. The y-axis is represented as r/R, where R is the radius of the artery. The parabolic appearance of these curves indicates that the velocity of the fluid is greatest at the center line of the artery, and that it reduces asymptotically to zero at the walls of the artery. A higher hematocrit will increase the effective viscosity of blood which will result in increased resistance to flow through the artery for the same pressure gradient. Therefore, the blood velocity decreases as the hematocrit level increases. The results clearly demonstrate the inverse relationship between hematocrit and blood velocity, and highlight the large effect that hematocrit has on arterial hemodynamics and flow efficiency. In addition, the figure shows that as the hematocrit level increases the peak axial velocity also decreases, as well as being decreased over all parts of the pulse cycle. This is due to the fact that there is an increase in the effective viscosity of blood at higher hematocrit levels; this causes an increase in flow resistance so that under a given pressure gradient less fluid flows per unit area than would be possible if there were fewer red blood cells in solution.

The temporal variation of the peak axial velocity is shown graphically for a range of hematocrit values from 0.35 to 0.55 in figure (2). On the x-axis is time, and on the y-axis is the maximum axial velocity at the centerline of the artery.

International Journal of Advanced Research in Computer and Communication Engineering
Impact Factor 8.471 ⁜ Peer-reviewed & Refereed journal ⁜ Vol. 15, Issue 8, August 2026
DOI: 10.17148/IJARCCE.2026.15808

Both figures show that for all hematocrit levels, the axial velocity exhibits a periodic sinusoidal variation characteristic of arterial blood flow. During systole, i.e., during contraction of the heart, the centerline velocity increases to a maximum, and after systole, or relaxation of the heart, it returns to a lower value. For all hematocrit levels, the maximum centerline velocity was reached approximately 0.2 sec into systole. As expected, both figures show that as hematocrit increases, peak axial velocity decreases uniformly over the entire pulse cycle. Thus, using either figure, we can conclude that high concentrations of red blood cells are detrimental to efficient arterial blood transport.

The relationship between the flow rate and hematocrit is illustrated in figure (3). The amount of volume flowing through an artery at any one time changes with hematocrit throughout a cardiac cycle. Volume (flow) rate is shown on the vertical axis; time is shown along the horizontal axis. Both graphs show the oscillations from each heartbeat. Volume flow peaks rapidly during the systolic phase of the cardiac cycle approximately .2 seconds into it. Then they drop down to zero approximately .6 seconds later. Then they start to increase again before the onset of the next pulse. Viscosity of blood increases as hematocrit increases. Therefore, there is increased resistance to blood flow, which results in lower volumes of blood flow for the same oscillating pressure gradient. Although a greater hematocrit may result in lessened volume flow rate amplitudes, the cyclic characteristics of a pulsatile waveform remain intact. A high hematocrit limits arterial capacity to transport blood, and thus increased blood viscosity hinders blood circulation and generates additional work for the cardiovascular system.

Figure (4) depicts how hematocrit changes along the length of an artery for various radial distances from the lumen or inside surface (r/R=0.00), to the outer surface (r/R=0.95) of an artery. The x axis represents location along an artery (length), whereas the y axis represents hematocrit as a function of those locations. In every radial section, hematocrit increases as one travels downstream and eventually reaches a constant level (asymptote) somewhere near the end of the artery. This indicates that the distribution of cells within an artery has reached equilibrium. High levels of hematocrit occur closest to the center line of an artery, where low levels occur closest to the interior surface of the arterial wall. The development of hematocrit distributions occurs because red blood cells tend to migrate radially towards the center line of an artery in response to shear stress; thereby creating a "rich in cell" core that surrounds a "poor in cell," or plasma layer, adjacent to the arterial wall. Also apparent in this figure is that the rate at which hematocrit is increasing is greater for each radial position as one moves closer to the center line than moving farther away. This illustration shows that both the longitudinal position and radial position have a significant effect upon the distribution of hematocrit, and therefore provides additional insight into how cell components move through and are distributed within arteries during pulsatile blood flow.

The data in figure (5) shows a steady decline in plasma concentration along the vessel length at all radial locations. The fact that there are ongoing processes of transporting plasma components and consuming them by the vascular endothelium indicate a continuous process of diffusion throughout the entire length of the artery. It can also be observed from the figures that the highest plasma concentration occurs along the central axis of the vessel (i.e., at r = 0) and the lowest plasma concentration always occurs immediately adjacent to the vessel wall. The radial distribution of plasma within the vessel occurs because red blood cells move toward the center of the vessel. Therefore, a “cell-rich” region of high hematocrit exists centrally with a "plasma-poor" region surrounding it. Along the wall of the vessel, a very thin plasma-depleted zone exists. The rate of plasma removal clearly slows down as you approach the end of the vessel. At this point, the plasma concentrations across all radial points begin to equilibrate. These data demonstrate that radial position and axial distance each have significant roles in defining how plasma moves through the arterial system. These studies highlight additional reasons why we should understand how convection, diffusion, and cellular transport interact to influence plasma movement under conditions of pulsatile blood flow in arteries.

As shown in figure (6), cellular concentration also varies along the vessel length for each radial location examined in this study. At all radial locations studied, there was a progressive increase in cellular concentration as one traveled down the vessel length. This trend indicates that as blood cells are carried down the artery, they accumulate and redistribute themselves throughout the vessel. Similar to plasma concentration data, higher cellular concentrations were observed along the centerline than at any other radial location studied. Conversely, lower cellular concentrations were measured closer to the vascular wall. These trends are consistent with previously described mechanisms involving shear-induced migration of red blood cells toward the central region of the vessel; ultimately producing a cell rich core and a cell-depleted boundary layer along the wall. Cellular concentrations increased rapidly at the beginning of the vessel and then stabilized or reached equilibrium values farther down stream. In addition to showing that cellular redistribution processes reach an equilibrium state throughout most of the arterial length, it was evident from these measurements that radial position has a significant effect upon cellular component transport and accumulation within the arterial lumen. Therefore, these studies demonstrate that convective transport and shear induced migration are two critical mechanisms controlling cellular concentration distributions in vessels subjected to pulsatile flow.

International Journal of Advanced Research in Computer and Communication Engineering
Impact Factor 8.471 ⁜ Peer-reviewed & Refereed journal ⁜ Vol. 15, Issue 8, August 2026
DOI: 10.17148/IJARCCE.2026.15808

A radial profile of hematocrit versus normalized axial location z/L for the range $0.00 \leq z/L \leq 1.00$ is presented in figure (7). The radial positions on the x axis are measured as fractions of the radius (R) of the vessel. Therefore, they range from r/R = 0.00 at the centerline to r/R = 1.00 at the vessel wall. The y axis represents the local hematocrit for each point on the plot. At every axial location, the hematocrit will be largest at the centerline and decrease radially outward towards the arterial wall. This forms a cell rich-core in the center of the artery and a cell depleted-plasma layer near the wall. As you move downstream, the hematocrit near the center line slightly increases. However, the hematocrit near the wall does not increase much so there is an increased radial gradient as the axial distance continues to grow. It is likely these trends can be explained by shear-induced migration of red blood cells from areas of higher shear stress (the area immediately adjacent to the arterial wall) to areas of lower shear stress (the area in the middle of the artery). The plasma concentrations shown in Figure 6.8 show how the plasma levels change along the length of the artery for a number of radial locations (from r/R = .00 [center line] to r/R = .95 [the arterial wall]). As indicated by the decreasing plasma level along the length of the artery at each of these locations, there is clearly continuous transfer and redistribution of plasma occurring through out the pulsatile arterial blood flow. Plasma levels are also higher near the center line than they are near the wall of the artery. These trends are consistent with the movement of red blood cells to the center of the vessels resulting in an alteration in the local distribution of plasma and a tendency to form a central core with high amounts of red blood cells and lower plasma levels, with a peripheral area that has lower amounts of red blood cells and higher amounts of plasma. There is a rapid drop in the plasma level from the inlet, followed by a gradual decline towards the outlet. It appears that this type of transport will eventually approach steady-state conditions as it continues further down stream. Since radial differences in plasma levels tend to decrease with increasing distance from the inlet due to a combination of convective and diffusive processes, the concentration profiles appear to be converging at larger axial distances. Therefore, this data illustrates that both axial location and radial position have significant influences on plasma transport; therefore, illustrating that pulsatile flow, diffusion and cellular redistribution can cause coupled effects to affect plasma concentration in the arterial lumen.

V. CONCLUDING REMARKS

A complete model of mathematical transport was built to explain both the movement of blood plasma and cellular components, in response to the pulse wave generated by the beating heart. This model links the effects of hematocrit on blood viscosity, the pulsatile motion of blood flow (Navier-Stokes) , convection/diffusion transport of plasma molecules, and the migration of red blood cells in shear, into a single mathematical theory. The solution of this system can be obtained analytically or through simulation using computer methods. Both types of methods were used to simulate all aspects of the pulsatile flow within an artery; such as velocity profiles, volumetric flow rates, hematocrit levels, plasma concentrations, cellular concentrations, and wall shear stresses. The results show that increased levels of hematocrit result in higher apparent viscosities in blood, which lead to decreased velocities, reduced flow rates and greater resistances to circulation. In addition, the simulations demonstrated the existence of a cell rich central region and a plasma depleted peripheral region as a result of red blood cell migration due to the pulsatile nature of blood flow. Plasma concentration decreased throughout the length of the artery as a result of convective, diffusive and uptake at the walls processes. Conversely, the concentration of cells increased throughout the length of the artery until equilibria is reached. Thus these results provide evidence of the high degree of interaction between blood rheological properties and the mechanisms of mass transport and also highlight the importance of hematocrit in controlling hemodynamic parameters within arteries.

REFERENCES

[1]. Abidin, S. N. A. M. Z., Jaafar, N. A., and Ismail, Z. (2021). Herschel–Bulkley Model of Blood Flow Through a Stenosed Artery with the Effect of Chemical Reaction on Solute Dispersion. *Malaysian Journal of Fundamental and Applied Sciences*, 17(4), 457–474.

[2]. Ahmad, R., Ali, A., and Ashraf, M. (2019). Steady Flow of a Power-Law Fluid Through a Tapered Non-Symmetric Stenotic Tube. *Applied Mathematics and Nonlinear Sciences*, 4(1), 255–266.

[3]. Ahmad, R., Ali, A., and Ashraf, M. (2021). An Analytical Approach to Study the Blood Flow Over a Nonlinear Tapering Stenosed Artery in a Carreau Fluid Model. *Complexity*, 2021, Article ID 6628143.

[4]. Ahmed, M., Khan, S., and Ali, F. (2025). Application of Mathematical Models for Blood Flow in Aorta and Coronary Arteries. *Applied Sciences*, 15(10), 5748.

[5]. Akbar, N. S., Nadeem, S., and Mekheimer, K. S. (2016). Rheological Properties of Reiner–Rivlin Fluid Model for Blood Flow Through a Tapered Artery with Stenosis. *Journal of the Egyptian Mathematical Society*, 24(1), 138–142.

[6]. Ali, A., Ahmad, R., and Ashraf, M. (2021). Mathematical Modeling and Parametric Investigation of Blood Flow Through a Stenosed Artery. *Applied Mathematics and Mechanics*, 42, 1675–1684.

International Journal of Advanced Research in Computer and Communication Engineering

Impact Factor 8.471 ⁜ Peer-reviewed & Refereed journal ⁜ Vol. 15, Issue 8, August 2026

DOI: 10.17148/IJARCCE.2026.15808

[7]. Bessonov, N., Sequeira, A., Simakov, S., Vassilevskii, Y., and Volpert, V. (2016). Methods of Blood Flow Modelling. *Mathematical Modelling of Natural Phenomena*, 11(1), 1–25.

[8]. Hussain, A., Khan, M., and Ali, S. (2026). Computational Analysis of Blood Flowing Through an Artery with Stenosis and Dilatation. *Scientific Reports*, 16, Article 12830953.

[9]. Kim, J., Lee, D., and Park, S. (2026). Toward Efficient Fluid–Structure Interaction Modeling in Patient-Specific Arteries Using Smoothed Particle Hydrodynamics. *Computer Methods in Biomechanics and Biomedical Engineering*, 29(4), 415–432.

[10]. Kumar, A., and Sharma, P. (2025). A Review on Non-Newtonian Mathematical Models for Blood Flow Through Stenosed Arteries. *International Journal of Mathematics Trends and Technology*, 72(3), 84–94.

[11]. Okafor, C., Bello, A., and Yusuf, M. (2026). Mathematical Modeling of the Impact of Temperature and Elevated Sickle Cell Concentration on MHD Blood Flow Through a Porous Atherosclerotic Channel. *Mathematics and Mathematical Analysis*, 11(2), 15–31.

[12]. Reddy, S., Kumar, P., and Singh, R. (2025). Dual-Rheological Model and Finite Element Simulation of Hemodynamics Through a Multiple Stenotic Artery with Nanodrug-Eluting Stent. *Scientific Archives of Biomedical Research*, 6(2), 101–118.

[13]. Riahi, D. N., and Orizaga, S. (2024). On Modeling Arterial Blood Flow with or Without Solute Transport and in Presence of Atherosclerosis. *AIMS Biophysics*, 11(1), 66–84.

[14]. Zhang, Y., Zhao, H., and Feng, J. (2023). Numerical Investigation of Red Blood Cell Migration in Microvascular Bifurcations. *Biomechanics and Modeling in Mechanobiology*, 22(4), 1251–1268.

[15]. Zhao, M. (2026). Pulsatile Flow Dynamics in Biomedical Engineering. *Physics of Fluids*, 38(3), 031302.